ADVANCES IN ATMOSPHERIC SCIENCES, VOL. 30, NO. 4, 2013, 1025–1038

# Airborne Measurements of the Impact of Ground-based Glaciogenic Cloud Seeding on Orographic Precipitation

MIAO Qun*[1] (缪 群) and Bart GEERTS[2]

[1]*Department of Applied Mathematics, Ningbo University, Ningbo* 315211

[2]*Department of Atmospheric Science, University of Wyoming, Laramie, Wyoming* 82071*, USA*

(Received 26 June 2012; accepted 3 September 2012)

**ABSTRACT**

Data from *in situ* probes and a vertically-pointing mm-wave Doppler radar aboard a research aircraft are used to study the cloud microphysical effect of glaciogenic seeding of cold-season orographic clouds. A previous study (Geerts et al., 2010) has shown that radar reflectivity tends to be higher during seeding periods in a shallow layer above the ground downwind of ground-based silver iodide (AgI) nuclei generators. This finding is based on seven flights, conducted over a mountain in Wyoming (the Unites States), each with a no-seeding period followed by a seeding period. In order to assess this impact, geographically fixed flight tracks were flown over a target mountain, both upwind and downwind of the AgI generators.

This paper examines data from the same flights for further evidence of the cloud seeding impact. Composite radar data show that the low-level reflectivity increase is best defined upwind of the mountain crest and downwind of the point where the cloud base intersects the terrain. The main argument that this increase can be attributed to AgI seeding is that it is confined to a shallow layer near the ground where the flow is turbulent. Yet during two flights when clouds were cumuliform and coherent updrafts to flight level were recorded by the radar, the seeding impact was evident in the flight-level updrafts (about 610 m above the mountain peak) as a significant increase in the ice crystal concentration in all size bins. The seeding effect appears short-lived as it is not apparent just downwind of the crest.

**Key words**: glaciogenic cloud seeding, orographic snowfall, cloud radar

**Citation**: Miao, Q., and B. Geerts, 2013: Airborne measurements of the impact of ground-based glaciogenic cloud seeding on orographic precipitation. *Adv. Atmos. Sci.*, **30**(4), 1025–1038, doi: 10.1007/s00376-012-2128-2.

## 1. Introduction

In the run-up to the Beijing Olympic Games, it was observed that "China has one of the largest programmes for weather modification in the world" (Qiu and Cressey, 2008). While weather modification efforts, in particular cloud seeding, appear to have been successful during the 2008 Beijing Olympic Games, there is little robust scientific evidence in support of successes claimed both in China and elsewhere. "... weather modification is one of those areas in which science can have an immediate and obvious benefit for society" is further argued (Qiu and Cressey, 2008).

Two cloud seeding effects are postulated to increase precipitation at the surface. The dynamic effect refers to the invigoration of deep convection, such as the thunderstorms targeted during the 2008 Beijing Olympic Games. This effect is attributed to the sudden release of latent heat as supercooled water freezes. The static effect is purely cloud-microphysical: in cold clouds, it refers to the initiation or acceleration of the Bergeron process by ice nuclei such as silver iodide (AgI) crystals or by dry ice. The Bergeron (or Bergeron–Findeisen) process is based on the difference in saturation vapor pressure at the surfaces of liquid water and ice. This difference peaks at −12°C. In warm clouds, the static seeding effect refers to the facilitation of collision-coalescence growth of droplets, typically by the injection of large, hygroscopic aerosol particles.

It is remarkable that notwithstanding numerous targeted field campaigns, in particular in the United

*Corresponding author: MIAO Qun, miaoqun@nbu.edu.cn

© China National Committee for International Association of Meteorology and Atmospheric Sciences (IAMAS), Institute of Atmospheric Physics (IAP) and Science Press and Springer-Verlag Berlin Heidelberg 2013

States, Israel, Australia, and China, the effectiveness of cloud seeding in enhancing precipitation remains uncertain (National Research Council, 2003). Notwithstanding this uncertainty, many private and public interests continue to support the seeding of clouds to enhance precipitation, which simply points to the high potential benefit, given the cost of water in water-limited regions. Operational seeding programs exist in many countries, including China, targeting both deep convection and stratiform clouds. Some seeding programs have been in operation for several decades. Some studies of surface precipitation enhancement have shown positive results, others did not obtain any statistically significant changes. The main problem with the experimental verification of precipitation enhancement is the high level of "noise" in naturally precipitating cloud systems, compared to the magnitude of the seeding signal (Garstang et al., 2005). Natural variability is especially challenging for deep convection.

If there is any chance of obtaining robust evidence for the effect of seeding on precipitation, relatively shallow orographic clouds must be targeted, since such cloud systems can be remarkably long-lived and steady (e.g., Grant, 1974), and they contribute significantly to the total precipitation in some regions (e.g., Roe, 2005). Both warm and cold orographic clouds have been studied. This paper focuses on cold orographic clouds. Some recent studies have shown that glaciogenic seeding of cold orographic clouds does indeed increase precipitation (Huggins, 2007; Geerts et al., 2010; Manton and Warren, 2011). The concept of glaciogenic seeding of orographic clouds is simple: clouds that rise rapidly over a mountain range typically contain numerous supercooled liquid water droplets. In continental airmasses rich with cloud condensation nuclei, these droplets will remain close to 10–15 micron in diameter, and not many droplets will be large enough (before reaching the mountain crest) to trigger precipitation formation by the collision-coalescence process. Ice nuclei are relatively rare in the atmosphere, especially at temperatures above about −15°C. In a mixed-phase cloud, ice crystals grow at the expense of droplets, mainly by vapor diffusion if the droplets are small. This is the basis for glaciogenic cloud seeding, whereby ice nuclei such as AgI particles are injected into a cloud, with the objective to maximize the conversion of liquid water into precipitating snow before the flow has crested the mountain range.

The efficacy of glaciogenic seeding of non-precipitating supercooled stratus clouds, decoupled from the earth surface, has been demonstrated long ago (e.g., Schaefer, 1946). It is far more difficult to demonstrate precipitation enhancement in naturally precipitating clouds that drape over mountains. Such clouds are more complex mainly because of boundary-layer turbulence (Geerts et al., 2011) and because ice particles can result naturally from interaction with the underlying terrain (Rogers and Vali, 1987). Yet such clouds are important because they produce much of the precipitation in arid, mountainous regions. For instance, glaciogenic cloud seeding has long been conducted in the Tian Shan range in western China, to enhance the water supply to the adjacent Tarim Basin (Abdulla et al., 2005). Altering the ice nucleation process in such clouds also alters other microphysical processes such as riming, leading to poorly understood changes both in cloud composition and in surface precipitation.

Several studies have attempted to document the cloud microphysical chain of events following AgI seeding of orographic clouds both in the USA (e.g., Super and Boe, 1988; Deshler et al., 1990; Huggins, 2007) and in China (e.g., Liu et al., 2005; Li, 2006). These studies generally examined individual cases rather than a population of storms. They confirm that it is very difficult to ascertain the effective transport of the AgI nuclei over the target area, and to relate changes in liquid water content (LWC) and ice particle size distributions in cloud to seeding activity. Given the complexities of chain-of-events studies, and the statistical uncertainty of outcome-focused randomized experiments, progress in understanding the impact of ground-based glaciogenic cloud seeding is most likely through measurements of cloud microphysical processes by means of modern remote sensing instruments, in particular profiling cloud radars.

This study uses airborne profiling W-band Doppler radar data as well as *in situ* data. Cloud radars have a high sensitivity and fine spatial resolution. At mm-wave frequencies, the signal becomes attenuated in heavy precipitation, but this is not a problem for the typically light snowfall rates from orographic clouds. The nadir view (see Fig. 2 in Geerts et al., 2006) provides radar data within ∼30 m of the ground, whereas the commonly used ground-based scanning radars can only "look" above the terrain peaks. The ability to look close to the terrain is important in the evaluation of ground-based seeding since the effect of seeding should be largely confined to the turbulent planetary boundary layer (PBL) (Geerts et al., 2011).

This study builds on Geerts et al. (2010), who use composite profiling cloud radar data from several flights, each with a no-seeding period followed by a seeding period, to show that radar reflectivity was higher near the ground during the seeding periods. The flight tracks were geographically fixed and identical in the no-seeding and seeding periods, so the

difference cannot be attributed to the terrain. The objective of this study is to further explore the data from 7 flights, used in Geerts et al. (2010), to examine the impact of glaciogenic cloud seeding. The composite data presented herein will shed some light on the cloud microphysical processes that lead to an alteration of precipitation due to AgI seeding of shallow orographic clouds.

Section 2 describes the data sources, and section 3 describes the atmospheric conditions during the flights. Section 4 illustrates some transects of airborne data across the target mountain. The dispersal of AgI nuclei in the boundary layer is discussed in section 5. The relationship between radar reflectivity and snow rate is examined in section 6. Composite reflectivity patterns are presented in section 7. Further evidence that the observed reflectivity change can be attributed to AgI seeding can be found in section 8, and the main findings are summarized in section 9.

## 2. Data sources

A series of five geographically-fixed aircraft tracks was flown repeatedly in winter storms in the vicinity of ground-based AgI generators in the Medicine Bow Mountains (MBM) of Wyoming, on a total of seven flight days in early 2008 and early 2009 (Fig. 1). These generators were operated as part of the Wyoming Weather Modification Pilot Project (WWMPP) (Breed et al., 2013)[a]. The MBMs are about 30-km across and 1500-m high above the surrounding plains (Fig. 1). The aircraft, the Wyoming King Air (WKA), carried in situ cloud microphysics probes, the Wyoming Cloud Radar (WCR), and the Wyoming Cloud Lidar (WCL). The WCR is a sensitive 94 GHz (3 mm) Doppler radar with zenith- and nadir-pointing antennas (http://www.atmos.uwyo.edu/wcr/). The WCL is a 0.355 micron elastic polarization backscatter lidar, also with zenith- and nadir-pointing antennas Wang et al. (2009).

The seven flights are summarized in Table 1, which is explained next. The flight tracks in rows 1 and 2 of Table 1 are numbered and locations are labeled as shown in Fig. 1. The flight-level liquid water content (LWC) in row 3 is inferred from a Gerber PVM-100 probe. The ice particle concentration in row 4 is the sum of the 2D-C and 2D-P concentrations, with a minimum particle size of 50 micron. The LWC and particle probe concentrations are averaged in cloud only (FSSP concentration at least 50 $cm^{-3}$). The mean fallspeed of hydrometeors in rows 5 and 6 is based on a comparison between the air vertical velocity measured by the gust probe, and the mean WCR particle vertical motion measured at the nearest radar gate above and below the aircraft, at a range of ∼120 m from the aircraft. The WCR reflectivity at 60 m above the surface in row 7 is averaged in units of $Z$ for all flight legs and then expressed in dB$Z$ units in Table 1. The surface snowfall rate in row 9 is measured by a Vaisala VRG101 gauge in 2008 and a Geonor T-200B gauge in 2009 at the target site near Brooklyn Lake (Fig. 1). The ice nucleus concentration in row 10 is measured with an acoustic ice nucleus counter (Langer, 1973) located at the same target site. The liquid water path in row 11 is derived from a two-channel (23 and 31 GHz) radiometer located at Cedar Creek (Fig. 1), with an

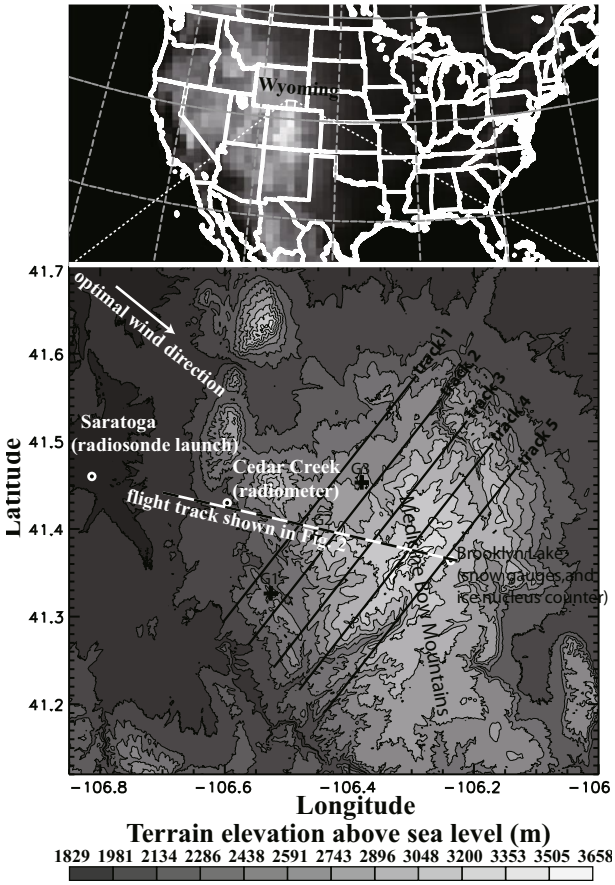


**Fig. 1.** Terrain map of the Medicine Bow Mountains in the Rocky Mountains, USA, showing the AgI generator sites (G1–G3), the surface measurement sites, and the five fixed flight tracks approximately normal to the wind. The upper map shows the location of this region within the USA. The flight level was maintained at about 4267 m above sea level (∼607 m above the mountain peak) for all tracks.

[a]Breed, D., R. Rasmussen, B. Lawrence, B. Boe, T. Deshler, C. Weeks, and S. Landolt, 2013: Evaluating winter orographic cloud seeding: Design of the Wyoming weather modification pilot project (WWMPP). *Bull. Amer. Meteor. Soc.*, in review.

**Table 1.** Summary of the 7 flight days. On four of the seven days, highlighted in bold, the static stability was particularly low.

| flight date | **11 Feb 2008** | **25 Feb 2008** | 18 Feb 2009 | 20 Feb 2009 | **10 Mar 2009** | **25 Mar 2009** | 30 Mar 2009 |
|---|---|---|---|---|---|---|---|
| **flight pattern** (see Fig. 1 for track identification) | | | | | | | |
| 1. no-seeding track sequence | **5-4-3-2-1** | **5-4-3-2-1** | 5-4-3-2-1 | 5-4-3-2-1 | **5-4-3-2-1** | **5-4-3-2-1** | 5-4-3-2-1 |
| | **5-4-3-2-1** | **5-4-3-2-1** | 5-4-3-2-1 | 5-4-3-2-1 | | | |
| 2. seeding track sequence | **5-4-3-2-1** | **5-4-3-2-1** | 5-4-3-2-1 | 5-4-3-2-1 | **5 times** | **5 times** | 4 times |
| | **5-4-3-2-1** | **5-4-3-2-1** | 5-4-3-2-1 | | **5-4-3** | **5-4-3** | 5-4-3 |
| **aircraft data** (averages for all passes over tracks 2-5) | | | | | | | |
| 3. average flight-level LWC in cloud (g $m^{-3}$) | **0.23** | **0.16** | 0.09 | 0.15 | **0.17** | **0.23** | 0.13 |
| 4. average flight-level ice particle concentration ($l^{-1}$) | **11** | **12** | 13 | 29 | **22** | **23** | 35 |
| 5. no-seed flight-level particle fallspeed (m $s^{-1}$) | **1.19** | **0.99** | 0.80 | 1.04 | **0.91** | **1.02** | 0.80 |
| 6. seed flight-level particle fallspeed (m $s^{-1}$) | **1.04** | **0.93** | 0.70 | 0.95 | **0.78** | **0.80** | 0.72 |
| 7. WCR -20 dBZ echo top height (m MSL) | **5408** | **5826** | 4697 | 6379 | **4092** | **6101** | 5100 |
| 8. WCR reflectivity at 60 m above the ground (dB$Z$) | **5.4** | **8.2** | 6.4 | 9.3 | **0.7** | **5.9** | 7.4 |
| 9. corresponding snow rate, assuming S=0.11 $Z^{1.25}$ (Matrosov, 2007) (mm $h^{-1}$) | **0.51** | **1.17** | 0.69 | 1.60 | **0.13** | **0.59** | 0.93 |
| **surface data** (averages during full flight period, except for ice nucleus concentration, which is an average during the seed period only) | | | | | | | |
| 9. water-equivalent snow rate at Brooklyn Lake (mm $h^{-1}$) | **0.60** | **0.32** | 1.01 | 1.17 | **0.22** | **0.66** | 0.31 |
| 10. ice nucleus concentration at Brooklyn Lake ($l^{-1}$) | **N/A** | **45** | 11 | ∼100 | **∼100** | **6** | 70 |
| 11. radiometer liquid water path at Cedar Creek (mm) | **0.06** | **N/A** | 0.08 | 0.06 | **0.03** | **0.12** | 0.02 |
| **Saratoga sounding data** (radiosonde released 115 minutes after aircraft take-off at Saratoga (Fig. 1)) | | | | | | | |
| 12. mean wind speed (m $s^{-1}$) | **15** | **12** | 14 | 15 | **21** | **14** | 11 |
| 13. mean wind direction (°) | **317** | **293** | 300 | 293 | **272** | **265** | 323 |

**Table 1.** (Continued)

| flight date | **11 Feb 2008** | **25 Feb 2008** | 18 Feb 2009 | 20 Feb 2009 | **10 Mar 2009** | **25 Mar 2009** | 30 Mar 2009 |
|---|---|---|---|---|---|---|---|
| 14. mean wind direction offset from flight track shown in Fig. 1 (°) | **12** | **−25** | 4 | 3 | **−9** | **−11** | 7 |
| 15. Brunt-Väisälä frequency ($10^{-2}$ s$^{-1}$) | **0.51** | **0.15** | 0.78 | 0.76 | **0.52** | **0.00** | 0.61 |
| 16. Froude number | **1.9** | **5.0** | 1.04 | 1.2 | **2.6** | $\infty$ | 1.1 |
| 17. Richardson number | **0.7** | **0.2** | 8.1 | 2.4 | **0.4** | **0.0** | 3.5 |
| 18. lifting condensation level (LCL) (m MSL) | **2719** | **2782** | 2630 | 2314 | **2896** | **2618** | 2807 |
| 19. LCL temperature (°C) | **−9** | **−7** | −10 | −8 | **−19** | **−7** | −16 |
| 20. temperature at the level of the AgI generators (°C) | **−9** | **−7** | −10 | −10 | **−17** | **−8** | −15 |

antenna pointing such that it measures liquid water above the MBM (91° azimuth from north, 10° elevation angle). This slant path is converted to a zenith one, i.e. it represents the vertically integrated liquid water. Rows 12–17 represent averages between ground level and the elevation of Medicine Bow Peak. The wind direction offset listed in row 14 is positive if the wind direction is clockwise relative to the flight direction. It is zero if the wind direction is normal to the five flight tracks (from 309°). The mean temperature at the elevation of the generators (listed in row 20) is estimated from the Saratoga sounding. The elevation of the three generators ranges between 2752–2946 m, and the mountain peak is at 3660 m.

Three AgI generators were used. These generators, and all others used in the WWMPP project, were off for at least four hours before WKA take-off. On each of the seven flights, the generators remained off ("no-seed") for the first one or two hours, and they were on ("seed") for the rest of the flight period (Table 1). Four flight tracks (#1 to #4, see Fig. 1) were on the upwind (northwesterly) side of the mountain, one (#5) was on the lee side. The first leg was upstream of the three AgI generators, and the last four were downstream, at distances ranging from 2 to 15 km from the generators at each of the legs' closest point. A radiosonde was released from Saratoga (mapped in Fig. 1) two hours after each aircraft take-off time.

A total of 44 "no-seed" (70 "seed") passes were made along the four downstream legs on the seven flights; the sequence of these passes is given in Table 1. The experimental design is intended to minimize differences between the seed and no-seed samples due to terrain or weather variability. A randomized design with some flights taking place entirely during seed operations, and others without any seeding, would have been ill-advised in this case, given the small number of flights (7) and the natural variability between storms.

## 3. Weather conditions during the flights

In all but one of the seven cases, a persistent winter storm was present without frontal passage during the duration of the flight, typically four hours long (Geerts et al., 2010). In all cases, the temperature was low enough to activate most AgI crystals: it was −7°C or colder at the level of the AgI nuclei generators, located about 500 m below the mountain top (Table 1). The wind was relatively strong wind in all cases (>10 m s$^{-1}$) (Table 1). The ideal wind direction was northwesterly, specifically the direction normal to the five flight tracks (from 309°, Fig. 1), a direction which is roughly aligned with the terrain slope. The real wind departed a little from this direction (Table 1), but the

orientation and length of the tracks allowed for significant wind direction departures that did not preclude encountering the AgI plumes somewhere along the flight track.

The synoptic situation in all but one of the 7 cases was post-frontal with little baroclinicity. One exception is 20 February, 2009, when a cold front passed during the flight. Low-level clouds generally were present over the MBM and other mountains in the vicinity.

We estimate the depth of each storm from the average height of the −20 dB$Z$ WCR echo top, listed in Table 1. If multiple −20 dB$Z$ echo tops are present, the highest continuously "connected" top is selected. The "connection" requires vertically continuous radar echoes above the minimum detectable signal (i.e. the noise level plus one standard deviation), which is about −28 dB$Z$ at a range of 1 km. In other words, an upper-level echo layer is ignored only if it does not measurably seed the clouds below with ice crystals. The echo top generally was relatively shallow, only about 1.5–4.5 km above the local ground elevation, according to WCR reflectivity profiles (Table 1). The average echo top height during the seven flights was only 1712 m above mountain top level. Generally echo tops were higher on the upwind side, and lower on the lee side, due to subsident flow there (Fig. 2b).

To ascertain that the upstream airmass did indeed ascend over the mountain, we calculate the bulk Froude number ($Fr$), defined as the wind speed $U$ divided by the Brunt-Väisälä frequency $N$ and the height $H$ of Medicine Bow Peak above the upstream plains:

$$Fr = \frac{U}{NH} \,, \tag{1}$$

here $U$ and $N$ are computed using upwind sounding data from the surface to mountain top height. $N$ is computed as the dry (moist) frequency below (above) the cloud base (defined as the lifting condensation level, LCL). Table 1 shows that $Fr$>1 on each of the seven days. This implies that the low-level flow was unlikely to be deflected around the mountain, but rather went over the mountain (e.g., Smolarikiewicz et al., 1988). This is confirmed by ice nucleus (IN) counter measurements at Brooklyn Lake, a high-elevation site in the lee of the mountain crest (Fig. 1). IN concentrations far exceed the "background" IN concentration (Table 1), starting shortly after the generators were turned on, on each of the 6 flight days that the IN counter functioned. The acoustical IN counter (Langer, 1973) was tuned to detect all IN that activate at temperatures above about −20°C. Any background concentration of natural IN was examined by means of IN counter measurements on several clear, unseeded days in the winter of 2008-09. On these days, the IN concentration was less than 1 per liter. Thus the observed high IN concentrations during the second half of the WKA flights can be attributed to AgI nuclei. Note that AgI nuclei can be depleted by nucleation or scavenging, and subsequent precipitation before reaching the Brooklyn Lake site.

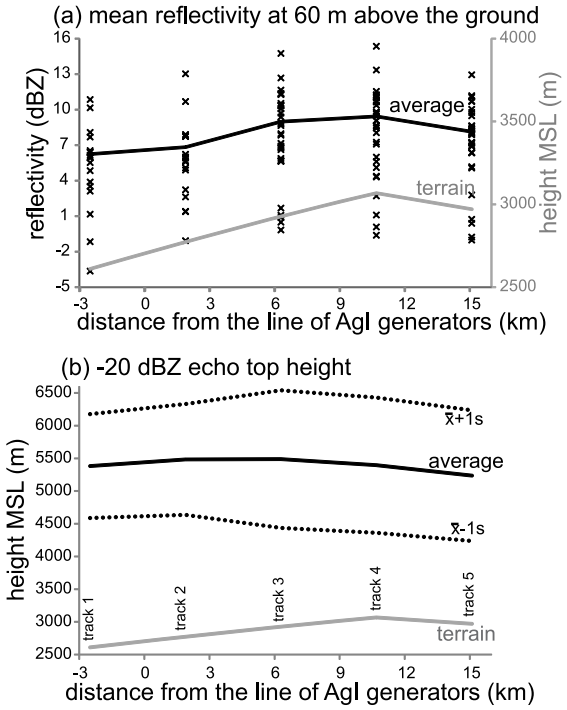


**Fig. 2.** (a) Mean WCR reflectivity just above the terrain, and (b) mean −20 dB$Z$ echo top height, for the five tracks shown in Fig. 1, for the 7 flights listed in Table 1. The crosses in (a) represent individual flight legs. In (b) only the ±1 standard deviation from the mean is shown. All flight legs are included irrespective of the seeding action.

The typically high Froude number was the result of the case selection criteria, which favored strong winds and low stability near the surface. The static stability below mountain top level was generally rather low. On four of the seven days, highlighted in bold in Table 1, the static stability was particularly low, resulting in some cumuliform cloud tops and convective-scale vertical velocities over the mountain, as illustrated in Geerts et al. (2011). On those days the vertical shear of the wind was rather strong, such that the bulk Richardson number ($Ri$) was close to zero (Table 1). A low local $Ri$ value implies little resistance to vertical exchange by turbulence. We compute $Ri$ as:

$$Ri = \frac{N^2}{\left(\frac{\Delta V}{\Delta Z}\right)^2} \,, \tag{2}$$

where $\Delta V/\Delta Z$ is the magnitude of the wind shear between the mixed layer (50 hPa deep) and mountain top level.

On all seven days, the cloud base (estimated as the LCL) was at or below the elevation of the AgI generators. It snowed continuously, but not heavily, during all flights over the mountain, according to the WCR profiles and snow gauge data from a sheltered site at Brooklyn Lake (Table 1). The average water-equivalent snowfall rates were light, between 0.22 and 1.17 mm $h^{-1}$ at the Brooklyn Lake site, and between 0.13 and 1.60 mm $h^{-1}$ according to the average WCR reflectivity measured along the five flight tracks at the lowest level uncontaminated by the surface (about 60 m above ground level) (Table 1). The Brooklyn Lake snow gauge recorded a slightly lower snowfall rate during the first part of the seven flights (no seeding) than during seeding periods of the flight times (0.59 vs. 0.64 mm $h^{-1}$). The difference is insignificant given the uncertainties in snowfall measurement, especially in a windy place, and given the few cases with a total of just 18.3 hours of flight data. Detailed snow gauge data analyses is reserved for the WWMPP, which has over 100 carefully selected cases each four hours long (Breed et al., 2013). The snow gauge, WCR reflectivity, and satellite IR cloud top data (not shown) all indicate relatively steady conditions during all but one flight (the exception is 20 February, 2009, when a cold front passed during the flight).

A lower mean reflectivity is observed along track 1. The highest values are along track 4 which is close to the terrain crest, although there is much variability between flights (Fig. 2a). This "orographic effect" is significant: between track 1 and track 4, the average snowfall rate ($S$) increases by a factor of 2.5, assuming the relationship $S$=0.11 $Z^{1.25}$ (Matrosov, 2007), where $Z$ is radar reflectivity (units: $mm^6$ $m^{-3}$) and $S$ is average snowfall rate (units: mm $h^{-1}$).

The cloud liquid water content at flight level was rather low, less than 0.25 g $m^{-3}$ on all days (Table 1). This is consistent with a rather low liquid water path in the orographic cloud, as estimated by a passive microwave radiometer on the upwind side (Cedar Creek, Fig. 1). Values of ∼0.1 g $m^{-3}$ were commonly observed also at low flight levels upwind of the Sierra Nevada (Deshler et al., 1990).

## 4. Sample of radar profile data

To illustrate the potential of WCR and WCL data for the study of cloud microphysical processes over mountains, an example is shown in Fig. 3. This flight leg was along the wind, across the five-track "ladder" pattern shown in Fig. 1. The low-level wind was westerly at ∼14 m $s^{-1}$, the cloud base height 2.6 km MSL, and the cloud base temperature −7°C (Table 1). Note the shallow clouds on the left side, well below flight level, detected by the WCL: the rapid attenuation of the lidar backscatter power (Fig. 3c) indicates the presence of droplets. The radar reflectivity values suggest that some ice already is present in these shallow clouds (Fig. 3a). A streamer of reflectivity appears to emerge from the surface between 1606:30 UTC and 1606:00 UTC (x axis is time). The cloud top is well-defined and no deep clouds are advected from the west. Turbulent eddies mark the PBL (Fig. 3b). Snow grows towards the mountains crest, according to the radar and lidar profiles. A high depolarization ratio (Fig. 3d) indicates non-spherical particles, i.e. ice. The lack of rapid attenuation and high depolarization ratio values indicate that droplets are absent on the lee side of the crest. A further analysis of the lidar data is beyond the scope of this paper. Flight-level particle probe data (Figs. 3e and f) record a portion of the orographic cloud and precipitation region.

The WCR vertical velocity data indicate that during all flights turbulent mixing occurred within the PBL, as can be seen in Fig. 3b and especially in another example (Fig. 4b). The turbulent motion produces vertical velocity variations larger in magnitude than the mountain-scale flow. On the more stable flight days, the PBL top could be readily identified as the top of the turbulent layer, and the WCR vertical velocity pattern suggests a decoupling of the turbulent PBL from the stratified orographic flow pattern aloft, as in Fig. 4b. On less stable days small-scale turbulent updrafts often merged to form larger convective updrafts reaching the tops of clouds marked by cumuliform edges. This is examined in detail in Geerts et al. (2011).

## 5. Boundary-layer turbulence and AgI dispersal

The turbulence can be expected to effectively mix the AgI nuclei over the depth of the PBL. These nuclei have a negligible fallspeed. We derived the 2D flow pattern for the along-wind flight leg in Fig. 4, using WCR dual-Doppler synthesis below flight level. The WCR dual-Doppler synthesis package is described in Damiani and Haimov (2006). A value of 1.0 m $s^{-1}$ has been added to the vertical component to remove the average fallspeed of the hydrometeors and retain the 2D air flow (Fig. 4c). The fallspeed is estimated as in Geerts et al. (2011); average values are shown in Table 1. During seeding periods the fallspeed estimates are slightly lower, suggesting relatively more snow growth by deposition rather than by accretion.

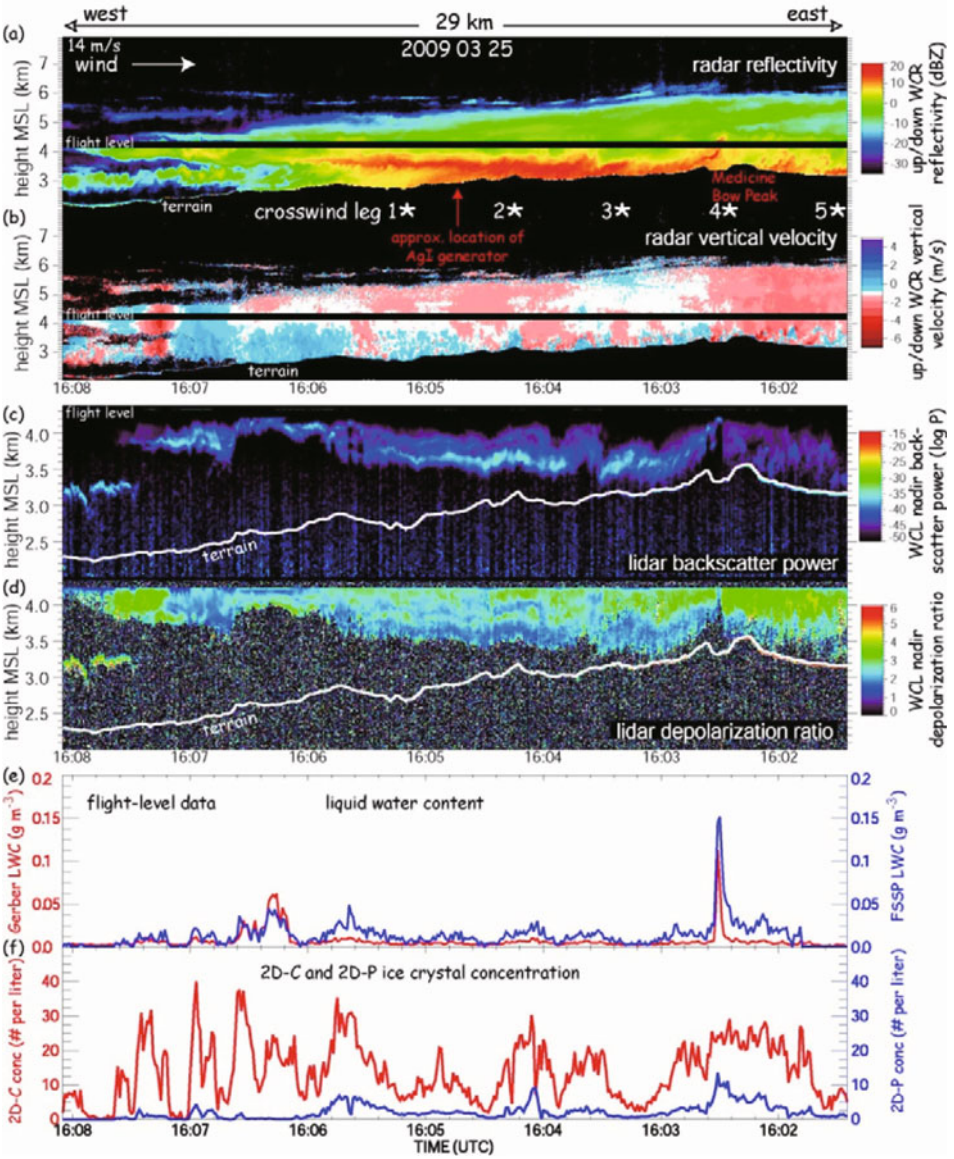


**Fig. 3.** An along-wind transect of Wyoming Cloud Radar (WCR) data (panels a and b) and Wyoming Cloud Lidar (WCL) data (panels c and d), flown along the mean wind between 1601–1608 UTC on 25 March 2009. The flight level is within the black belt in panels (a) and (b). This belt is the radar blind zone, centered at flight level. The lidar data are shown only below flight level. The radar data readily reveal the terrain profile. This profile was added in the nadir lidar transects. Also shown are flight-level estimates of liquid water content from the Gerber PVM-100 and the FSSP probes (panel e) and of ice particle concentrations from the 2D-C and 2D-P probes (panel f).

The sample flow pattern in Fig. 4c suggests that typical air streamlines starting near the surface at the approximate location of the AgI generators do not reach the PBL top before reaching the mountain crest. However if we examine the spread of actual trajectories around this snapshot of streamlines, using the probability density function of the WCR dual-Doppler winds ($u$, $w$) within the PBL, then we find that some air parcels emerging from near the AgI generators may reach the PBL top and even the flight level. This is consistent with several previous studies that recorded evidence of AgI seeding plumes and/or of a tracer gas released at the AgI generators at flight level (e.g., Huggins, 2007), and with recent airborne acoustic ice nucleus counter measurements in clear air over the MBM (not shown).

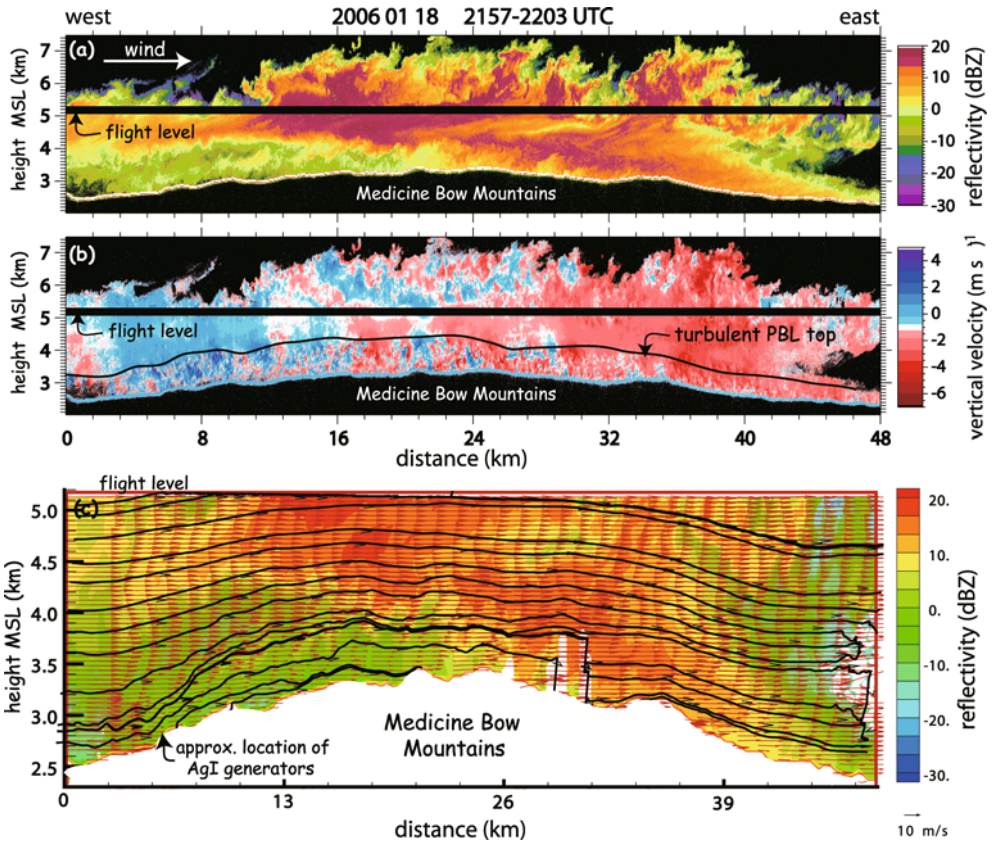


**Fig. 4.** WCR data for an east-west transect on 18 January 2006 across the Medicine Bow Mountains, flown along the westerly wind. (a) WCR reflectivity; (b) WCR vertical velocity; (c) WCR dual-Doppler winds (red vectors) and streamlines (black arrows) on top of radar reflectivity (color field) for roughly the same section as (a) but below flight level only. A value of 1.0 m $s^{-1}$ has been added to the vertical component to remove the average fallspeed of the hydrometeors.

## 6. W-band reflectivity and snowfall rate

The key strength of the dataset analyzed herein is the radar reflectivity data in very close proximity to the terrain. At 94 GHz (W-band) the radar echo is dominated by ice crystals scattering in the Mie regime. This scattering process is complex and highly dependent on crystal shape, orientation, and size distribution (Matrosov, 2007). Instead of making assumptions about these parameters and computing the theoretical liquid-equivalent snow rate ($S$) corresponding with the observed 94 GHz reflectivity ($Z$), we relate the observed WCR $Z$ (units: $mm^6$ $m^{-3}$) near flight level to the observed liquid-equivalent $S$ (units: mm $h^{-1}$) at flight-level (Fig. 5). The $Z$ value is obtained as an average of the closest radar gates above and below the aircraft. These gates are at a radar range of about 120 m. The snow rate $S$ is computed from the snow size distributions given by two PMS probes (2D-C and 2D-P), the hydrometeor density, and the observed particle terminal fall velocity (Table 1). The hydrometeor density is estimated from particle size according to the relationship for dry snow particles in Rasmussen et al. (2003).

The snow rates in the orographic clouds generally were quite light at flight level, but a sufficient number of high snow rate values were encountered to reveal a $Z-S$ relationship that reasonably corresponds with one of the theoretical relationships by Matrosov (2007). That paper actually shows several relationships, giving a range $Z-S$ correspondences, owing to uncertainties in scattering model assumptions, in particular the snowflake's mass, fallspeed, and aspect ratio. The average observed $Z-S$ relationship reasonably matches the theoretical relationship, esp. for the 2D-P probe. This applies both during seeding legs and without seeding. Because the seeding effect is most likely felt at flight level along tracks 4 and 5 only, we focused on those tracks only during seeding, and the correspondence between observations and theory is still good (Fig. 5). For the purpose of our argument, it is sufficient to note that the snow rate tends to in-

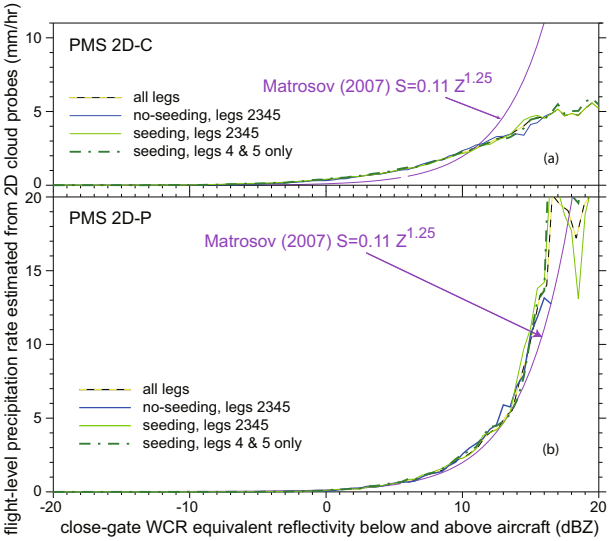


**Fig. 5.** Flight-level precipitation rate ($S$) against near-flight-level radar equivalent reflectivity ($Z$) for all 7 flights. The precipitation rate is estimated from the snow size distributions given by the (a) 2D-C and (b) 2D-P probes, an assumed hydrometeor density, and the measured mean particle terminal fall velocity. The abscissa shows the average WCR equivalent reflectivity in the nearest gate above and below the aircraft, at a range of ∼120 m. Four lines show the observed mean $S$ value for each $Z$ bin for (dashed line) all passes over tracks 2–5, (solid blue) no-seed passes only, (solid green) seed passes only, and (dash-dot line) seed passes only over tracks 4 and 5. The fifth (purple) line shows the best-matching theoretical Z-S relationship according to Matrosov (2007).

crease significantly at WCR reflectivity values over 5 to 10 dB$Z$. While such values are rare at flight level, they are far more common near ground level.

## 7. Frequency by altitude displays

In order to assess the effect of glaciogenic seeding, Geerts et al. (2010) composited WCR data collected along flight tracks downwind of the AgI generators in the form of a frequency-by-altitude display (FAD) (Yuter and Houze, 1995). Here we use the same technique, but we focus on the effect of seeding supercooled water clouds that develop as the air ascends over the mountain. A FAD is derived as follows: all WCR data collected along straight and level flight legs (Fig. 1), excluding the aircraft turns between the legs, are remapped as a function of height above ground level (AGL). The occurrences of reflectivity (or vertical velocity) values are then counted in bins with dimensions of 0.5 dB (0.1 m s$^{-1}$) and 30 m, for all range gates and all profiles. The vertical resolution (30 m) matches the WCR range resolution. The counts in each bin are then normalized by the total count of all occurrences in all bins. Examine, for instance, the reflectivity FAD for all WCR profiles where the terrain is below cloud base, during no-seeding, for all seven flights (Fig. 6a). The summation of all bin values in this panel equals 1.0. Figure 6b displays the same, during seeding. The normalized bin values in Fig. 6b are subtracted from those in Fig. 6a to yield Fig. 6c. The "data presence" curves in Figs. 6a and b are the percentage of WCR range gates with reflectivity values above the noise level (−25 dB$Z$) at any height AGL. A nearly 100% data presence was achieved near the ground, especially closer to the mountain crest (Figs. 6d and e), indicating that it snowed almost everywhere at most times during the flights. The rapid decline in data presence above ∼2 km AGL indicates that the storms were rather shallow.

The depression in the "data presence" curves between 1 and 2 km is an artifact due to the radar blind zone centered at flight level. This blind zone can be seen in Fig. 3 and Fig. 4. The flight level was constant (about 4267 m above sea level), but the aircraft height above ground level clearly was not. This artifact clearly also affects the FADs, but it does not affect the distribution or mean value at any height. The WCR reflectivity was hardly attenuated by water vapor, by liquid water, or by strong particle scattering, because it was quite cold (Table 1), the LWC was low at flight level (Table 1), and the path-integrated reflectivity was relatively weak (Fig. 6), respectively.

Geerts et al. (2010) examined the reflectivity FAD for all seven flights and the four tracks downwind of the generators and found a low-level (below 1 km) dipole in the difference FAD, with positive values (a higher probability during seeding) between 10–15 dB$Z$, and negative values (reduced probability during seeding) at lower reflectivity values. The average enhancement of reflectivity during seeding was found to be 1.0 dB near the ground, which translates into a 25% snowfall rate enhancement, according to the relationship $S$=0.11 $Z^{1.25}$ (Matrosov, 2007).

The key question regards cause and attribution. This dipole could be a chance effect due to natural variability. Certainly one cannot draw a definitive conclusion from just seven flights or a total sampling time of just 18.3 hours, seed and no-seed flight sections combined. Geerts et al. (2010) provide both statistical and physical arguments in favor of the attribution of this enhancement to AgI seeding. The three main physical arguments are (a) the depth of the dipole in the reflectivity difference FAD corresponds well to the depth of the turbulent boundary-layer mixing as evident from the WCR vertical velocity profiles (this matters be-

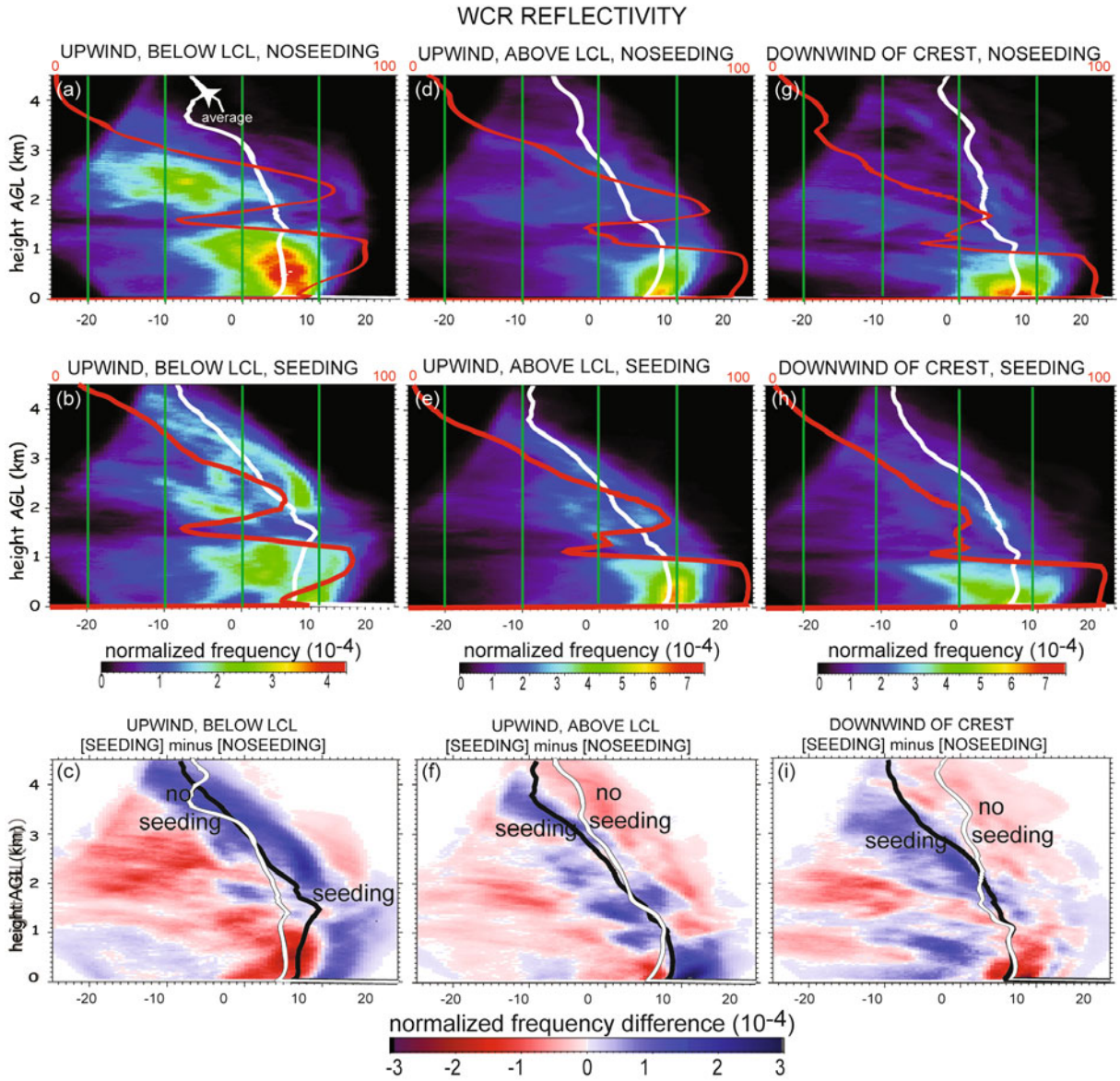


**Fig. 6.** Normalized FAD of WCR reflectivity ($Z$) for all flight tracks on 7 flights, during no-seeding (3 panels in the top row) and seeding conditions (middle row). Also shown are the mean reflectivity profile (white line) and the "data presence" (red line), i.e. the percentage of WCR range gates with radar echo as a function of height. The difference (seeding minus no-seeding), i.e. between the data in the middle row and the top row, is shown in the lower row, together with the respective average profiles (black and white lines). For the three panels on the left, the radar profiles were collected below the upwind cloud base (defined as the sounding LCL, see Table 1); the right column applies to radar profiles downwind of the mountain crest; and the middle column applies to radar profiles between the LCL and the crest.

cause the AgI seeding is ground-based, as discussed in section 5); (b) on less stable days with shallow but intense convective updrafts, the dipole in the reflectivity difference FAD is deeper and more intense; and (c) the low-level enhancement of high-reflectivity frequencies during seeding occurs notwithstanding the slightly deeper, more intense storm periods encountered during no-seeding periods.

## 8. Further physical evidence for a seeding effect

We now explore three arguments that provide further physical evidence for the attribution of the observed reflectivity difference to AgI seeding. The first argument is the strongest one. It regards the effect of seeding supercooled water clouds that form upwind

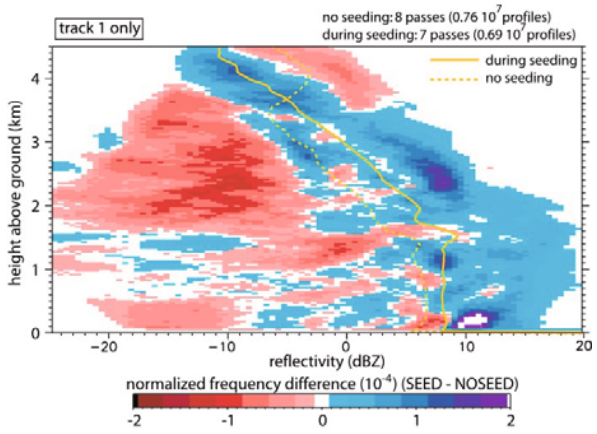


**Fig. 7.** The (seeding minus no-seeding) difference in normalized FAD of WCR reflectivity ($Z$) for all passes over track 1 only. Note that the composite reflectivity difference is based on the first four flight days only, because track 1 was not flown at all during seeding on the last three flight days (Table 1). The yellow dashed/solid lines represent the average reflectivity profiles.

of a mountain. If ice crystals are present, they will grow by deposition or accretion occurs as the air rises above the cloud base, which we estimate as the LCL from the upwind sounding. This growth tends to concentrate at rather low levels (e.g., Geerts et al., 2011). The intent of glaciogenic seeding is to accelerate this process by the injection of ice nuclei near cloud base. The AgI generators were located generally just above cloud base during the seven flights (Table 1), and 10-11 km from the mountain crest. In Fig. 6 the WCR profiles from all five flight tracks (Fig. 1) and all seven flights are separated by their location relative to the cloud base intersecting the mountain contour. Upwind of the cloud base/terrain intersection there is very little evidence of any seed effect (Figs. 6a–c), as expected. Higher reflectivity values tend to occur during seeding, but this seems to relate to a slightly more intense storm activity aloft during those periods. There may be some low-level enhancement, as turbulent mixing may carry AgI nuclei in this region to a level above cloud base.

Another region we isolated in the lee side. The exact location of the mountain crest depends on the wind direction. The low-level seed-effect dipole is not apparent downwind of the crest (Figs. 6g–i), suggesting that the AgI seeding effect is short-lived (Maybe there is still some residual seed effect, but it appears to be offset by more intense storm activity aloft during the no-seed period.)

A clear low-level dipole can be seen between the cloud base and the crest (Figs. 6d–f), so the seed-effect dipole reported by Geerts et al. (2010) really is concentrated in the region between cloud bases and crest, where the introduction of ice nuclei is expected to trigger snow growth. In short, strong low-level reflectivity enhancement occurs during seeding on the windward mountain side, just downwind of where cloud base intersects the terrain, and not (or much less) in the lee of the mountain or upwind of that intersection.

A second argument regards flight track 1, which was intended as a "control" track as it is located upwind of the three AgI generators (Fig. 1). This track was intended to ascertain any "pre-existing" (weather-related) difference between seed and no-seed periods. The "orographic effect" is as expected: the average reflectivity along track 1 is lower than along the four downstream legs (Fig. 2a), by a few dB$Z$ especially at low levels. There were significant stretches along track 1 without measurable ($> -25$ dB$Z$) echo below flight level.

Track 1 passes were excluded from the FADs in Geerts et al. (2010). The track 1 difference FAD (Fig. 7) reveals that storms were generally deeper and stronger during seeding, which agrees with the below-LCL composite difference (Fig. 6c). The surprise in Fig. 7 is the very shallow dipole, between 7 dB$Z$ and 11 dB$Z$. It is likely to be a signature of AgI seeding, but it is only ∼300 m deep. We hypothesize that this dipole signature is due to turbulent diffusion of AgI nuclei against the prevailing wind direction. A similar upstream diffusion has been found in large eddy simulations of ice nuclei released from model points matching the AgI generator locations in the MBM (R. Rasmussen and L. Xue, personal communication). Such upwind transport can be due to turbulence and/or to local terrain-driven circulations, such as drainage wind. Note that track 1 is just 2.5 km upwind of the line connecting the three generators. Thus track 1 is too close to the generators to serve as "control".

The third argument regards a confirmation of the seed effect using flight-level particle-probe data. The flight level generally was too high to be significantly affected by ground-based seeding, as discussed in section 5. It varies between 0.6 km and 2.1 km AGL with the most common level at 1.2 km AGL, as can be seen in the "data presence" curves in Figs. 6d–e. This mostly is above the region of reflectivity enhancement (Fig. 6f). There is no evidence for a reduction in supercooled liquid water during the seed periods, according to data from any of the four *in situ* probes (a FSSP drop size distribution probe, a Rosemount 871 FA icing probe, a Gerber PVM-100 probe, and a DMT-100 hot wire probe). Nor did the 2D-P and 2D-C ice particle concentrations increase significantly during seeding. The 2D-C data indicate a slight in-

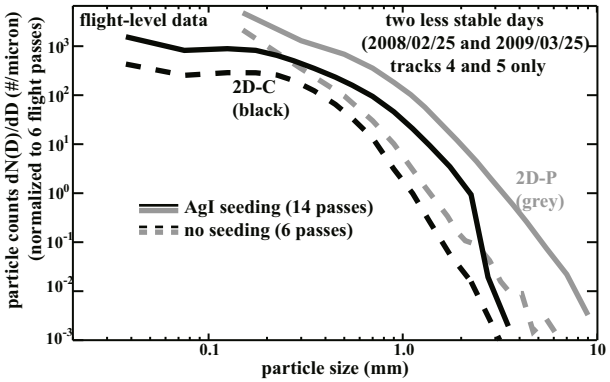


**Fig. 8.** Ice particle size distribution in updraft regions for all seed and no-seed passes over tracks 4 and 5 on the two days with lowest static stability. There were more seed passes than no-seed passes on these two days, thus the particle counts are normalized to allow a fair comparison.

crease in smaller ice particles (less than 0.5 mm in diameter) during seeding, but no increase in concentration of larger particles. The seed effect does become apparent in the data from the two flights with the lowest ambient stability, and with cumuliform clouds at and above flight level, and only along tracks 4 and 5, where the terrain is highest (Fig. 1) and thus the flight level AGL the lowest. For two such flights, we found substantially higher 2D-P and 2D-C particle concentrations in all size bins during the seeding periods along tracks 4–5. The seeding/no-seeding difference is largest if we further limit this sample to updraft regions only (Fig. 8). Convective mixing occurred over the depth of the cloud on these flights, resulting in a deeper reflectivity "seed-effect dipole" than that evident in Fig. 6f (Geerts et al., 2010).

A third uncertainty regards the small sample size. Caution is warranted given the limited number of storms sampled (7), and the limited flight times. The storms sampled represent a narrow region in the spectrum of precipitation systems in terms of stability, wind speed, storm depth and cloud base temperature.

This third weakness justifies further field research. In the winters of early 2012 and early 2013 we conducted 17 more WKA flights in southern Wyoming in an experiment called ASCII (AgI Seeding Cloud Impact Investigation), a collaborative effort with the National Center for Atmospheric Research and the University of Colorado. The WKA instrument suite and flight tracks were similar, but there was a Doppler-On-Wheels (DOW) dual polarization X-band scanning radar and a Ka-band profiling radar on the mountain crest downwind of the generators, plus a mountain research station with a host of instruments to measure the surface snowfall rate and the particle size distribution, and to image the ice crystals. The latter will provide more insight into the snow growth mechanisms, and will also enable us to refine the assumptions in the relationship between snowfall rate and reflectivity at W-band and other at radar frequencies.

## 9. Conclusions

This study examines the impact of ground-based glaciogenic seeding of orographic clouds on cloud microphysical processes. It builds on earlier work (Geerts et al., 2010) and provides further experimental evidence, mainly from vertically-pointing airborne radar data, that ground-based AgI seeding can increase the near-surface radar reflectivity in orographic snow storms. The reflectivity data are composited in frequency-by-altitude displays along geographically fixed flight tracks. Each of the seven flights used herein has a seeding period following a no-seeding period. An increase in reflectivity (and thus snowfall rate) during seeding is found within the turbulent boundary layer downwind of the AgI generators, in particular over the high terrain above cloud base. Such increase is absent on the leeward side, even though the winds were strong and the AgI generators were only ∼10 km upwind of the crest. This suggests that the seeding effect is rather short-lived. The flight level generally is too high to measure the seeding effect with *in situ* probes, but flight-level ice particle concentrations are significantly higher in cumuliform updrafts along the flight tracks over the highest terrain.

The results presented here are preliminary because just seven storms were sampled. The work also raises some questions, in particular regarding the relative role of diffusional and accretional snow growth in natural conditions, and the possibility of natural seeding from the ground. This work has been followed up with a longer field campaign in 2012 and 2013 under similar as well as more diverse weather conditions. In addition to the airborne probes, this campaign, referred to as ASCII (AgI Seeding Cloud Impact Investigation) included ground-based instruments, such as vertically pointing Ka-band radars and a X-band dual-polarization radar, and probes to measure ice particle size distribution, riming amount, and habits.

***Acknowledgements.*** The 7 WKA flights, radiosondes, and the data analysis were financed through the University of Wyoming Water Research Program. The operation of the AgI generators was supported by the WWMPP, which is funded by the State of Wyoming. The acoustical IN counter data were provided by Bruce BOE. YANG Yang assisted in the data analysis. The Brooklyn Lake snow rate and Cedar Creek radiometer data were provided by Dan

BREED. The ASCII campaign is funded by the National Science Foundation grant AGS-1058426. Dr. MIAO Qun is partially sponsored by K.C.Wong Magna Fund in Ningbo University.

## REFERENCES

Abdulla, R., X. Li, X. Wei, and W. Xu, 2005: Analysis of synthetic conditions favourable for artificial precipitation in Tianshan Mountain area. *Bimonthly of Xinjiang Meteorology*, **2**, 41–52. doi: cnki:SUN:XJQX.0.2005-02-008. (in Chinese)

Damiani, R., and S. Haimov, 2006: A high-resolution dual-Doppler technique for fixed multi-antenna airborne radar. *IEEE Trans. Geosci. Remote Sens.*, **42**, 3475–3489.

Deshler, T. D., W. Reynolds, and A. W. Huggins, 1990: Physical response of winter orographic clouds over the Sierra Nevada to airborne seeding using dry ice or silver iodide. *J. Appl. Meteor.*, **29**, 288–330.

Garstang, M., R. Bruintjes, R. Serafin, H. Orville, B. Boe, W. Cotton, and J. Warburton, 2005: Finding common ground. *Bull. Amer. Meteor. Soc.*, **86**, 647–655.

Geerts, B., R. Damiani, and S. Haimov, 2006: Fine-scale vertical structure of a cold front as revealed by airborne radar. *Mon. Wea. Rev.*, **134**, 251–272.

Geerts, B., Q. Miao, Y. Yang, R. Rasmussen, and D. Breed, 2010: An airborne profiling radar study of the impact of glaciogenic cloud seeding on snowfall from winter orographic clouds. *J. Atmos. Sci.*, **67**, 3286–3302.

Geerts, B., Q. Miao, and Y. Yang, 2011: Boundary-layer turbulence and orographic precipitation growth in cold clouds: Evidence from profiling airborne radar data. *J. Atmos. Sci.*, **68**, 2344–2365.

Grant, L. O., 1974: Weather modification, a pilot project: San Juan Mountain River Basin. Final Report to the United States Bureau of Reclamation. Contract 14-06-D-6467 to Colorado State University, 98pp.

Huggins, A. W., 2007: Another wintertime cloud seeding case study with strong evidence of seeding effects. *Journal of Weather Modification*, **39**, 9–36.

Langer, G., 1973: Evaluation of NCAR ice nucleus counter. Part I: Basic operation. *J. Appl. Meteor.*, **12**, 1000–1011.

Li, S., 2006: Case study of cloud and precipitation microphysics structure over Northwest China. *Meteorological Monthly*, **8**, 59–63.(in Chinese)

Liu, J., M. L. Li, T. Jiang, C. S. Mi, and Z. X. Chen, 2005: The preliminary study of the basic structure of precipitating stratus and precipitation potential in spring in Jilin Province. *Scientia Meteorologica Sinica*, **25**, 609–616. (in Chinese)

Manton, M. J., and L. Warren, 2011: A confirmatory snowfall enhancement project in the Snowy Mountains of Australia. Part II: Primary and associated analyses. *J. Appl. Meteor. Climatol.*, **50**, 1448–1458.

Matrosov, S. Y., 2007: Modeling backscatter properties of snowfall at millimeter wavelengths. *J. Atmos. Sci.*, **64**, 1727–1736.

National Research Council, 2003: *Critical Issues in Weather Modification Research.* National Academy Press, 123pp.

Qiu, J., and D. Cressey, 2008: Meteorology: Taming the sky. *Nature*, **453**, 970–974.

Rasmussen, R., M. Dixon, S. Vasiloff, F. Hage, S. Knight, J. Vivekanandan, and M. Xu, 2003: Snow nowcasting using a real-time correlation of radar reflectivity with snow gauge accumulation. *J. Appl. Meteor.*, **42**, 20–36.

Roe, G. H., 2005: Orographic precipitation. *Annual Review of Earth and Planetary Science*, **33**, 645–671.

Rogers, D. C., and G. Vali, 1987: Ice crystal production by mountain surfaces. *J. Climate Appl. Meteor.*, **26**, 1152–1168.

Schaefer, V. J., 1946: The production of ice crystals in a cloud of supercooled water droplets. *Science*, **104**, 457–459.

Smolarikiewicz, P. K., R. M. Rasmussen, and T. L. Clark, 1988: On the dynamics of Hawaiian cloud bands: Island forcing. *J. Atmos. Sci.*, **45**, 1872–1905.

Super, A. B., and B. A. Boe, 1988: Microphysical effects of wintertime cloud seeding with silver iodide over the Rocky Mountains. Part III: Observations over the Grand Mesa, Colorado. *J. Appl. Meteor.*, **27**, 1166–1182.

Wang, Z., P. Wechsler, W. Kuestner, J. French, A. Rodi, B. Glover, M. Burkhart, and D. Lukens, 2009: Wyoming cloud lidar: Instrument description and applications. *Optics Express*, **17**, 13576–13587. doi: 10.1364/OE.17.013576.

Yuter, S., and R. A. Houze, 1995: Three-dimensional kinematic and microphysical evolution of Florida cumulonimbus. Part II: Frequency distributions of vertical velocity, reflectivity, and differential reflectivity. *Mon. Wea. Rev.*, **123**, 1941–1963.